applied sciences

MDPI

Article

Studying the Impact of Diffuser Return Guide Vanes on the Energy Performance of a Multistage Centrifugal Pump

Jan Górecki [1], Kliment Klimentov [2,*], Gencho Popov [2], Boris Kostov [2] and Salaf Ibrahim [2]

[1] Faculty of Mechanical Engineering, Institute of Machine Design, Poznan University of Technology, 60-965 Poznan, Poland; jan.gorecki@put.poznan.pl
[2] Department of Heat, Hydraulics and Environmental Engineering, University of Ruse, 7017 Ruse, Bulgaria; gspopov@uni-ruse.bg (G.P.); bkostov@uni-ruse.bg (B.K.); sibrahim@uni-ruse.bg (S.I.)
* Correspondence: kklimentov@uni-ruse.bg

Abstract: The head, efficiency, and cavitation characteristics of centrifugal pumps are highly dependent on the velocity field in front of the impeller inlet. In multistage pumps, the velocity field in front of the second and each subsequent stage is determined by the shape (design) of the diffuser return guide vanes. This current work presents the results obtained by performing a numerical study using ANSYS CFX 14.0 to determine the impact of the shape (design) of diffuser return guide vanes on the head and coefficient of efficiency of one stage of a multistage centrifugal pump. Three RGVs with different Outlet angles are studied: α_6—original RGV with $\alpha_6 = 90$ deg, RGV1 with $\alpha_6 = 110$ deg and RGV2 with $\alpha_6 = 128$ deg. The results obtained after performing CFD modeling indicate that with one of the studied RGVs, the pump stage head increases by nearly 20%, while the hydraulic coefficient of efficiency remains almost constant. Applying entropy production theory is used to determine the impact of the various components of entropy production on the total head loss in the studied pump stage. The impact of the Outlet angle of the RGV on the velocity field of the flow in front of the next impeller (stage) as well as the RGV head is also analyzed. The numerical results of the original RGV are compared with the experimental data obtained from large-scale studies of pumps performed at the Laboratory of Hydraulic Machines of the University "Angel Kanchev" of Ruse, Bulgaria. When using the modified RGVs, the head curve of the original pump can be obtained by operating at a lower speed or with a smaller impeller diameter. This may lead to an overall increase in the energy efficiency of the machine, which could be explored as a future task.

Keywords: centrifugal pump; return guide vanes (RGVs); computational fluid dynamic (CFD)

Citation: Górecki, J.; Klimentov, K.; Popov, G.; Kostov, B.; Ibrahim, S. Studying the Impact of Diffuser Return Guide Vanes on the Energy Performance of a Multistage Centrifugal Pump. *Appl. Sci.* **2024**, *14*, 10991. https://doi.org/10.3390/app142310991

Academic Editor: Salvatore Vasta

Received: 28 September 2024
Revised: 22 November 2024
Accepted: 25 November 2024
Published: 26 November 2024

1. Introduction

Multistage centrifugal pumps are widely used in many industries, including energy, domestic water supply and agriculture, as part of fluid transport systems where high pressure (head) is required. It is well known that turbomachinery is one of the main consumers of electricity worldwide. According to Ref. [1], the world market volume for centrifugal pumps is in the order of USD 20 billion per year. The increasing demand for energy efficiency necessitates improvements in the components of these machines, which are significant energy consumers worldwide. In-depth research on this problem in Bulgaria has been performed at the University of Ruse. In Ref. [2], the author proposes a large-scale experimental and theoretical study concerning the return device of a multistage centrifugal pump 11MT32, manufactured by VIPOM, Vidin, Bulgaria. The studies are related to the determination of the impact of the geometry of the return guide vanes (RGVs) on the indicators of the studied stage as well as of the entire pump. The number of RGVs is equal to the number of Radial diffuser vanes downstream of the pump impeller. The vanes are profiled on arcs of circles.

The authors in Ref. [3] modeled the flow in two-, three- and four-stage centrifugal pumps using ANSYS CFX, applying the k − ε turbulence model. The numerical results

obtained are validated using data provided by the pump manufacturer. As a result of the study performed, the impact of the number of impeller blades, the number of vanes of the return device and the number of stages of the pump on its head, as well as the coefficient of efficiency and power, was determined.

In Ref. [4], the authors studied the possibility of reducing the overall size of a multistage centrifugal pump using a circumferential twisted return guide vane. The study is based on applying CFD modeling of the flow through a two-stage pump, using ANSYS FLUENT. A turbulence model of the type RNG $k-\varepsilon$ is used in this study. As a result, the authors propose replacing the existing six-stage pump with a four-stage pump that ensures the same head.

Considering Ref. [5], it is clear that the interaction between the impeller and guide vanes has the most significant impact on the energy loss and pump coefficient of efficiency. The results provided concern a numerical study of a 10-stage centrifugal pump. The method LES (Large Eddy Simulation) is used.

In Ref. [6], the authors presented an experimental study on the impact of the vanes of the reciprocating apparatus of a multistage pump on pump performance. It is found that the return vane, whose trailing edge is set at the outer wall radius of the downstream annular channel, which discharges the swirl-less flow, ensures a good pump performance. Additionally, the impeller blade is modified to obtain shock-free conditions at the inlet. The blade length of the modified impeller with the smaller blade inlet angle is slightly longer than that of the standard (original) impeller, and the modified impeller slightly improves the pump coefficient of efficiency.

In Ref. [7], a new method for profiling the guide vanes of the guide and return devices of a multistage centrifugal pump is proposed. Four types of two-dimensional and three-dimensional new vanes are presented, which, according to the authors of Ref. [7], lead to an increase in the pump efficiency. However, the study does not provide information on the results obtained after performing research on the operation of pumps with these newly developed vanes.

In Ref. [8], a method to optimize the design of a typical multistage centrifugal pump based on the energy loss model and Computational Fluid Dynamics (CFD) is proposed. External characteristic experiments are also performed to benchmark numerical simulations. It is found that reducing volumetric leakage and interstage leakage losses is the most effective technique for increasing the efficiency of standard centrifugal pumps.

In Ref. [9], a numerical study on the performance of a multistage centrifugal pump for different Radial diffuser shapes is performed. It is found that the differential head is lower when the return channel Outlet angle is 60 deg instead of 90 deg because of the pre-swirl at the diffuser Outlet. The turbulence model SST $k-\omega$ is used; however, no information is provided concerning the computational grid. Thus, it is not clear whether the results obtained are compared with the experimental data.

In Ref. [10], a numerical study of unsteady flow and time variation of pressure within a complete double-blade centrifugal pump is presented. For this purpose, a SST $k-\omega$ turbulence model is used, and the results obtained are validated using experimental data provided by the same authors. As a result, it is found that the rotor–stator interference between the impeller and volute is the main source of pressure pulsation.

A study in which five types of volute structures are designed is presented in Ref. [11]. FLUENT is used to determine the steady and unsteady calculation of the five volute structure models. It is found that the static pressure gradient distribution of the double-tongue volute centrifugal pump under various operating conditions is improved to varying degrees, and the low-speed region of the diffusion section is reduced. The numerical results obtained are then validated with experimental data.

The impact of leakages and balance holes on the performance of a multistage centrifugal pump has also been studied experimentally, as well as using CFD, in Ref. [12]. The relative difference between the CFD and experimental results is in the range of 1–10%. It is

found that balance holes reduce the hydraulic efficiency of the pump by increasing the leak flow, although it is important to reduce the axial forces of the pump shaft.

The impacts of wall roughness, impeller blades, and diffuser vanes on the performance of a one-stage centrifugal pump is studied in Refs. [13,14]. The studies are performed numerically, and the results are validated using experimental data. A turbulence model of the type $k-\varepsilon$ is used for this purpose. Thus, it is found that the pump stage head and brake horsepower increased as the height of impeller blades and diffuser vanes and the number of impeller blades increased. In addition, the higher wall roughness heights of the impeller and diffuser negatively affected the pump stage head, brake horsepower and efficiency. The impact of the surface roughness on the performance of a two-stage centrifugal pump is also studied in Ref. [15]. The study is performed using CFD simulations, and the numerical results are validated using experimental data obtained by the authors. It is found that surface roughness has the greatest impact on disk friction losses. In this regard, the authors in Ref. [15] recommend that the outer impeller surfaces, as well as the pump casing part surfaces, should be manufactured with the minimum possible values of roughness. For this aim, a standard $k-\varepsilon$ turbulence model and surface roughness of 1 μm is used.

In Ref. [16], a study concerning the development of a centrifugal pump for operation at high head and high flow rates is conducted. The first stage of the pump consists of a double-suction impeller. A twin volute is installed after the first impeller, and an inducer-type guide vane is installed between the first and second stages (ITGV). Numerical studies used to determine the pump operation by using ANSYS CFX are performed. In this case, a SST $k-\omega$ turbulence model is used. As a result of the numerical experiments performed, it is found that using the ITGV leads to a decrease in the circumferential velocity of the fluid but also improves the overall performance of the pump by diminishing the losses obtained in the second stage. The authors in Ref. [16] emphasize that the experimental validation of the results obtained is pending.

A numerical study on the flow in the return device of a multistage centrifugal pump is presented in Ref. [17]. The standard k-ε turbulence model is adopted as the turbulence model, and impeller rotation is simulated using the multiple reference frames (MRF) method. The results obtained concern the effects of the return channel blade curvature on reducing the recirculation of flow inside the return channel vanes of a multistage centrifugal pump. It is demonstrated that return channels with exit blade angles of 90 and 100° ensure the best performance in the head and efficiency of the pump among the considered return channels. In addition, these channels are used to remove the flow recirculation inside the return channel; hence, the efficiency of the pump can be increased by approximately 2%.

The impact of channel-diffuser blades on the energy performance of a three-stage centrifugal pump is studied in Ref. [18]. The research is numerical, and for accomplishing this study, ANSYS CFX is used. In this case, a k-ε turbulence model is applied. The analysis of the results obtained indicates that under the design condition, the flow loss in three-stage diffusers accounts for 60.23% of the total flow loss. The pump efficiency is maximum when the blade inlet angle is set to 12 degrees.

Through research conducted in the field of multistage centrifugal pumps, particularly in relation to the assessment of the impact of RGV on pump performance, it is evident that enhancing vane geometry remains an unresolved research issue. The advancement of computational techniques and software tools for the numerical modeling of fluid flows has made these studies significantly more cost-effective and accessible compared to experimental approaches. The reviewed studies have demonstrated enhancements in RVG geometry, primarily applicable to systems operating with a specific radial vane diffuser. As mentioned in Ref. [5], the diffuser effect on pump losses is considerable. A study comparing two different vane diffusers in combination with various RGVs in a multistage pump is presented in Ref. [2]. The study demonstrates that the head produced by the pump is lower than what is stated in the manufacturer catalog, despite the pump being manufactured with smaller clearances in the front impeller seal. This study aims to validate a two-stage CFD model of an 11MT32 pump using experimental data provided in Ref. [2]. A new

geometry for an RGV is designed, and a geometric model of the studied pump stages with this new geometry is created. A computational mesh is generated and numerical experiments are conducted using ANSYS CFX 14.0. Performance indicators for the studied pump stages with the new RGV geometry are obtained as a result. After conducting a comparative analysis of the results, it is clear that when using the modified vane, the studied stage achieves a higher head and operates with a higher hydraulic coefficient of efficiency compared to the original (standard) vane.

2. Computational Modeling

2.1. Pump Model

The object of study in this present work is one stage of a three-stage centrifugal type 11MT32 pump with a specific speed of $n_q = 22.6$ min^{-1}. This study is numerical and performed using ANSYS 14.0. Geometric models are established using the Design Modeler subroutine, while computational meshes are generated in the mesh subroutine of the ANSYS Workbench 14.0. The numerical simulations are accomplished by applying ANSYS CFX. A geometric model of the flow part (fluid region) of two of the pump stages is established. Each stage consists of an impeller, vane diffuser and RGV. The vane diffuser and the RGV are united in a common body, which is called Radial diffuser 1 for the first stage and Radial diffuser 2 for the second one, respectively. Both impellers are identical, have six blades each and do not have rear balance holes. The vane diffuser has eight vanes, which is the same number as the RGV. Due to limited computing resources, the impeller models represent 1/6 of a whole impeller, each containing one blade. The vane diffuser and RGV models make up 1/2 of the total elements with four vanes each. A diagram of the newly established geometric model is shown in Figure 1a,b, which displays the main sizes of a RGV. Table 1 presents the main geometric parameters of the pump stage studied, as well as the three RGVs studied.

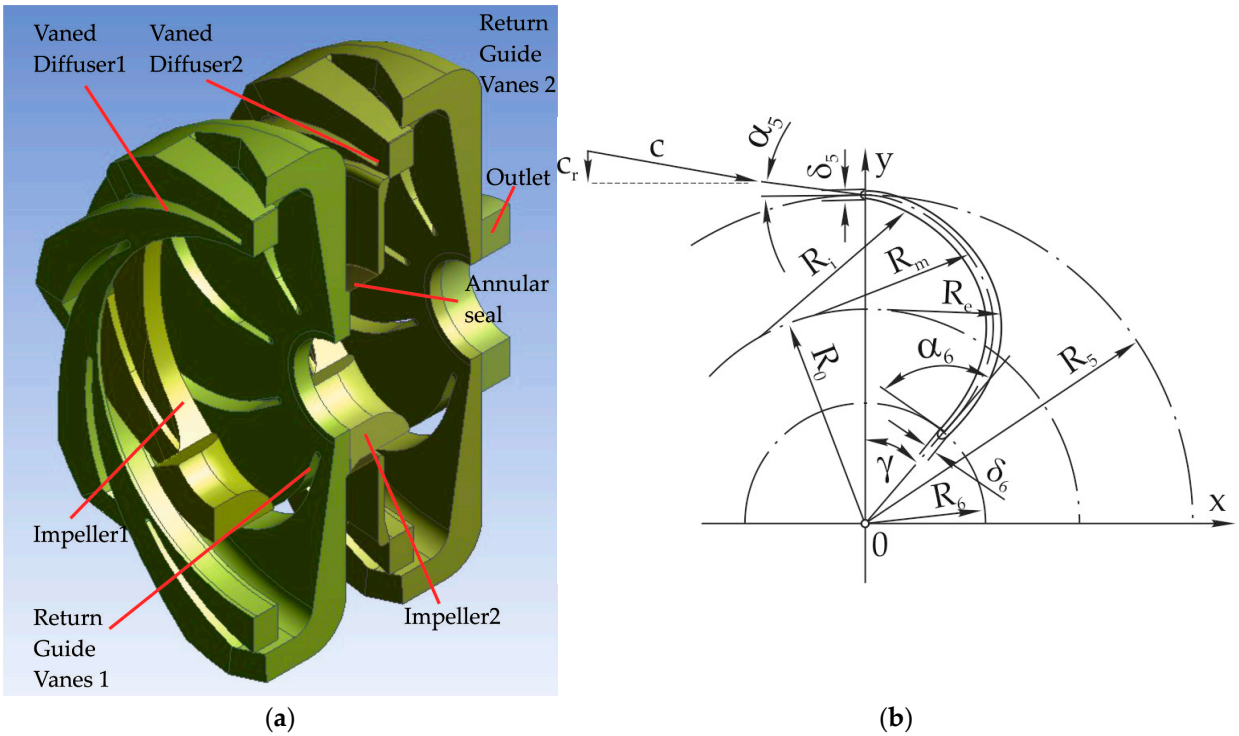

(**a**) (**b**)

Figure 1. Geometry of the studied object: (**a**) geometric pattern of the two stages created in Design Modeler; (**b**) geometric sizes of RGV.

Table 1. Basic geometric parameters of the pump stage studied.

Pump Element	Parameters	Symbol	Value
Impeller	Number of blades	z_{La}	6
	Inlet diameter (mm)	D_1	76.0
	Outlet diameter (mm)	D_2	168.0
	Outlet blade width (mm)	b_2	9.3
	Outlet angle (deg)	β_2	30
Radial Diffuser	Number of blades	z_{Le}	8
	Inlet diameter (mm)	D_3	170.0
	Outlet diameter (mm)	D_4	234.5.0
Original RGV	Radius at blade inlet (mm)	R_5	98.5
	Radius at blade outlet (mm)	R_6	42.5
	Angle at blade inlet (deg)	α_5	24
	Angle at blade outlet (deg)	α_6	90
	Placement angle (deg)	γ	27
	Initial radius (mm)	R_0	61.1
	Inner radius of the blade (mm)	R_i	46.1
	Outer radius of the blade (mm)	R_e	38.6
	Middle radius of the blade (mm)	R_m	41.3
	Thickness at blade inlet (mm)	δ_5	3.0
	Thickness at blade outlet (mm)	δ_6	2.0
RGV1	Radius at blade inlet (mm)	R_5	97.0
	Radius at blade outlet (mm)	R_6	44.0
	Angle at blade inlet (deg)	α_5	11
	Angle at blade outlet (deg)	α_6	110
	Placement angle (deg)	γ	24
	Initial radius (mm)	R_0	64
	Inner radius of the blade (mm)	R_i	-
	Outer radius of the blade (mm)	R_e	-
	Middle radius of the blade (mm)	R_m	34.0
	Thickness at blade inlet (mm)	δ_5	3.0
	Thickness at blade outlet (mm)	δ_6	2.0
RGV2	Radius at blade inlet (mm)	R_5	97.0
	Radius at blade outlet (mm)	R_6	44.0
	Angle at blade inlet (deg)	α_5	24
	Angle at blade outlet (deg)	α_6	128
	Placement angle (deg)	γ	11
	Initial radius (mm)	R_0	69.0
	Inner radius of the blade (mm)	R_i	35.9
	Outer radius of the blade (mm)	R_e	30.3
	Middle radius of the blade (mm)	R_m	32.3
	Thickness at blade inlet (mm)	δ_5	3.0
	Thickness at blade outlet (mm)	δ_6	2.0

The angle α_5 at the inlet of RGV1 is determined by the condition that the streamline at the inlet of the vane is tangent to the midline of the vane. The angle is calculated by applying the following equation:

$$\alpha_5 = \arcsin\frac{c_r}{c} \quad (1)$$

Velocity values for c and c_r are obtained after running a simulation using a diffuser without a RGV and a nominal pump operating mode with a flow rate of $Q = 11.39\ dm^3/s$ closest to the nominal one, $Q_n = 11\ dm^3/s$.

The inlet angle α_5 of RGV2 is set to be 24 degrees—equal to that of the original RGV.

The original vane angle α_6 is 90 degrees. Gulich [1], p. 510, recommends α_6 to be selected in the range of 94 deg to 96 deg. For RGV1, it is decided to be $\alpha_6 = 110$ deg, while for RGV2—$\alpha_6 = 128$ deg. In the authors' opinion, turning the flow against the rotation of the next impeller somewhat leads to an increase in its head.

The second pump stage is used in validating the results, as the experimental data obtained are based on studying this current pump stage. Furthermore, the simulation calculations with the three types of RGV are accomplished by using Radial diffuser 1 and Impeller 2 to establish the effect of RGV on the flow in front of the impeller inlet and the performance parameters of the pump stage.

2.2. Mesh Generation

Computational meshes are generated in the universal mesh generator within the ANSYS Workbench. Due to the complex geometry of the individual elements, an unstructured mesh with tetrahedral elements is used for Impeller 1, Impeller 2, Radial diffuser 1 and Radial diffuser 2. A structured mesh of hexahedral elements is generated for the Annular seal and Outlet. To perform mesh independence analysis, four meshes with different maximum sizes (largeness) of the tetrahedral elements are generated: Mesh1.4, with a maximum element size (MES) of 1.4 mm; Mesh1.3, with a MES of 1.3 mm; Mesh1.2, with a MES of 1.2 mm and Mesh1.0, with a MES of 1.0 mm. Fifteen layers of prismatic elements are generated on the walls of all fluid-flowed parts. The total thickness of the layers is 1.2 mm, with a growth rate of 1.1. Information about Numbers of Elements (NE) and Numbers of Nodes (NN) is provided in Table 2. Numbers of Elements represent the total number of volume elements used in designing the computational grid. Numbers of Nodes indicate the number of points used to connect the volume elements to each other. The volume elements can be of different types, such as tetrahedra, wedges, pyramids, hexahedral and polyhedral.

Table 2. Information about generated meshes.

Mesh	Numbers of Nodes	Numbers of Elements
Mesh1.4	2,356,423	6,106,712
Mesh1.3	2,591,368	6,460,859
Mesh1.2	2,990,093	7,496,622
Mesh1.0	4,246,084	10,775,711

2.3. Simulation Setup

As previously mentioned, the calculations are performed in ANSYS CFX 14.0. Impeller 1 and Impeller 2 are set to operate at a rotation speed of $n = 2920\ min^{-1}$. The working fluid is water with density $\rho = 997\ kg/m^3$. Radial diffuser 1, Radial diffuser 2, Annular seal and Outlet are stationary (fixed). The movement of the impellers relative to the fixed elements is simulated by applying Rotating Frames of Reference. The spatial discretization of the governing equations is based on the finite volume method. For the numerical solution of the RANS and URANS equation systems, the turbulent model $k - \omega$ SST, including the application of the Automatic Wall Function, is used. Simulation calculations are performed

under the Steady State condition and Transient Blade Row using Profile Transformation. The time step is 0.000171233 s, which corresponds to an angle of impeller rotation of 3°. High resolution is selected as the advection scheme. The transient scheme is Second Order Backward Euler, and thus, the turbulence numeric is high resolution. For convergence criteria, the Max Residual 5×10^{-4} is considered. The maximum number of iteration steps in each time step is set to 30.

Some specific (typical) boundary conditions are presented in Figure 2.

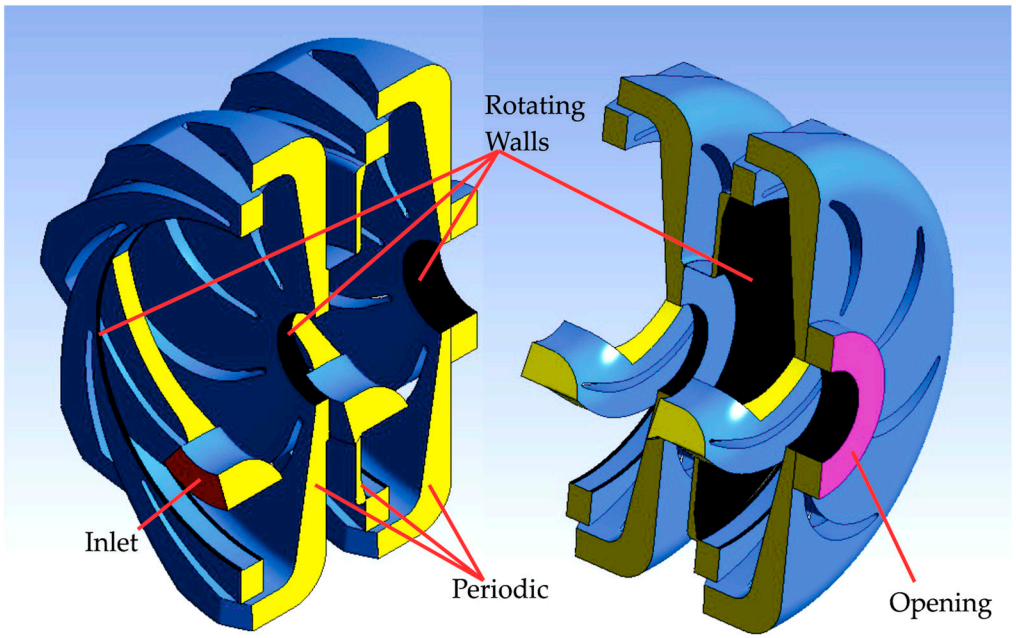

Figure 2. Boundary conditions.

At the inlet of Impeller 1, the inlet boundary condition is applied. Mass Flow Rate and Zero Gradient option for turbulence are set. The Outlet section of the Outlet element is set to the Opening condition, with a relative pressure of 8×10^5 Pa and the Zero Gradient option for turbulence. As parts of the impellers and diffusers are being modeled, a Rotational Periodicity Interface Model was used for some of the surfaces presented in Figure 2 (colored in yellow). To simulate the pump shaft rotation, the cover disk of Impeller 2 and the cylindrical surfaces at the Outlet of the impellers have conditions set for rotation (at speed $n = 2920\ \text{min}^{-1}$), as well as part of the surfaces of Radial diffuser 1 and Radial diffuser 2, whose surfaces are colored black in Figure 2. When applying the Steady State condition, the interface between the rotating impeller and the volute is set as stage. The interface model of Radial diffuser 1–Annular seal, Annular seal–Radial diffuser 2 and Radial diffuser 2–Outlet is General Connection without Frame Change/Mixing Model.

2.4. Entropy Production Theory

To numerically determine the indicators of the pump stage being studied, it is necessary to calculate the losses in the individual elements. The entropy generation theory is applied for this purpose. This theory has been used to analyze losses in centrifugal pumps in Refs. [19–23]. In Refs. [24,25], the authors demonstrate the implementation of entropy production calculation for turbulent shear flows in CFD.

In Ref. [23], the authors suggest calculating the power of the energy losses in a pump by applying the entropy generation theory and the absolute temperature, using the following equation:

$$P_{gen} = T\left(\Delta S_{gen,V} + \Delta S_{gen,T} + \Delta S_{gen,W}\right)\ (W) \quad (2)$$

where $T = const,\ (K)$ is the absolute temperature of the working fluid (water), which is assumed to remain constant in this case; $\Delta S_{gen,V}$ is the total entropy generation due to viscous diffusion; $\Delta S_{gen,T}$ is the total entropy generation due to velocity fluctuation; $\Delta S_{gen,W}$ is total entropy generation caused by the wall effect. The individual terms of Equation (9) are calculated as follows [23]:

$$\Delta S_{gen,V} = \int_V S_V dV,\ \left(WK^{-1}\right) \tag{3}$$

$$\Delta S_{gen,T} = \int_V S_T dV,\ \left(WK^{-1}\right) \tag{4}$$

$$\Delta S_{gen,W} = \int_a S_W dA,\ \left(WK^{-1}\right) \tag{5}$$

The rate of entropy generation due to viscous diffusion can be calculated as:

$$S_V = \frac{2\mu}{T}\left[\left(\frac{\partial \overline{u}}{\partial x}\right)^2 + \left(\frac{\partial \overline{v}}{\partial y}\right)^2 + \left(\frac{\partial \overline{w}}{\partial z}\right)^2\right] + \frac{\mu}{T}\left[\left(\frac{\partial \overline{v}}{\partial x} + \frac{\partial \overline{u}}{\partial y}\right)^2 + \right.$$
$$\left. + \left(\frac{\partial \overline{w}}{\partial x} + \frac{\partial \overline{u}}{\partial z}\right)^2 + \left(\frac{\partial \overline{v}}{\partial z} + \frac{\partial \overline{w}}{\partial y}\right)^2\right] \tag{6}$$

where $\mu,\ (Pa{\cdot}s)$ is the fluid dynamic viscosity; $\overline{u}$, $\overline{v}$ and $\overline{w}$ are Reynolds averaged velocity components in a Cartesian coordinate system.

The entropy generation rate due to velocity fluctuation can be determined by applying the following equation [23]:

$$S_T = \beta \frac{\rho \omega \kappa}{T} \tag{7}$$

where $\beta = 0.09$ is a constant; $\omega,\ \left(s^{-1}\right)$ is the turbulent eddy frequency; $k,\ \left(m^2/s^2\right)$ is the turbulent kinetic energy.

The rate of entropy generation, caused by the wall effect, can be calculated as follows [23]:

$$S_W = \frac{\vec{\tau}.\vec{v}}{T} = \frac{\tau_x u + \tau_y v + \tau_z w}{T} \tag{8}$$

where $\vec{\tau},\ Pa$ is the shear stress on the wall; $\vec{v},\ [m/s]$ is the velocity of the first grid near the wall. The parameters used in the estimation of S_v, S_T and S_W can be determined after solving URANS using the SST model. The determination of losses in the form of head can be performed by applying the following equation:

$$h_v = \frac{P_{gen}}{\rho g Q}\left(\frac{J}{N} \equiv m\right) \tag{9}$$

2.5. Mesh Independence

A mesh independence analysis is used for selecting a computing network. Numerical simulations are concluded for the four networks. The head H of the pump stage and the hydraulic coefficient of efficiency η_H, determined by established equations, are estimated as follows:

$$\eta_H = \frac{H}{H + h_{v,imp} + h_{v,diff}} \tag{10}$$

where $h_{v,imP}$ are the losses obtained in the studied impeller, determined by applying Equation (9); $h_{v,diff}$ is the losses in Radial diffuser 2, determined by applying Equation (9).

In Figure 3, the relationships of the types $H - NE$ and $\eta_H - NE$ are presented.

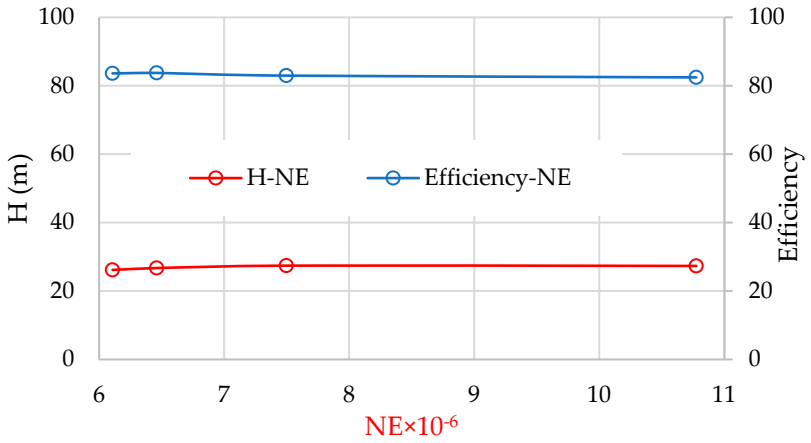

Figure 3. Variation in the head and hydraulic coefficient of efficiency of the pump stage is based on the Numbers of Elements (NE) in the computational network.

Table 3 presents the values of head and hydraulic coefficient of efficiency obtained during the calculations.

Table 3. Calculation results that are obtained using the generated meshes.

Mesh	H (m)	η_H (%)
Mesh1.4	27.3424	82.44878687
Mesh1.3	27.416	82.96281864
Mesh1.2	26.6984	83.73628451
Mesh1.0	26.172	83.59579139

The analysis of the data in Tables 1 and 2 clearly indicates that as the number of network elements increases from 7,496,622 to 10,775,711, which is close to a 44% increase, the head of the pump stage varies by 0.26 and the hydraulic coefficient of efficiency by 0.62%. Due to the minimal impact and to conserve computational resources, Mesh1.2 is selected for achieving the goals in this present study.

2.6. Experimental Data

The experimental data used to validate the results of the numerical simulations are published in Ref. [2]. This paper describes the experimental setup and method used for performing balance studies of multistage centrifugal pumps in detail. To evaluate the accuracy of the pump stage indicators, the Root Mean Square Error (RMSE) of the flow rate Q, head H, power H and the total coefficient of efficiency of the studied stage are determined. For one variant of the studies performed, with three parallel trials and a confidence probability of 0.95, the calculated RMSEs have the following values: $\mathrm{RMSE(Q)} = 0.0048$; $\mathrm{RMSE(H)} = 0.0472$; $\mathrm{RMSE(P)} = 0.0773$. At a confidence probability of 0.95 with three parallel trials, the total coefficient of efficiency error for the nominal operation mode is obtained as follows—$\Delta_\eta = \pm 0.477\%$.

Figure 4 represents a schematic of the experimental pump. The diagram is taken from Ref. [2] and is published with the permission of the author, P. R. Petrov. The focus of this study is the intermediate pump stage, which consists of an impeller, vaned diffuser, and return guide vanes. The primary goal of the first pump stage is to create the necessary conditions before entering the second stage. During the experiments, the impeller of the third stage is removed. The diagram indicates the points where water pressure is measured using corresponding manometers (pressure gauges), which are marked and numbered. The head H of the step is determined by readings from devices connected at points 2 (before the entrance of the tested stage) and 12 (after the exit of the tested stage). Additional

experiments are conducted to determine leakages through annular seals, and the results are published in Ref. [2].

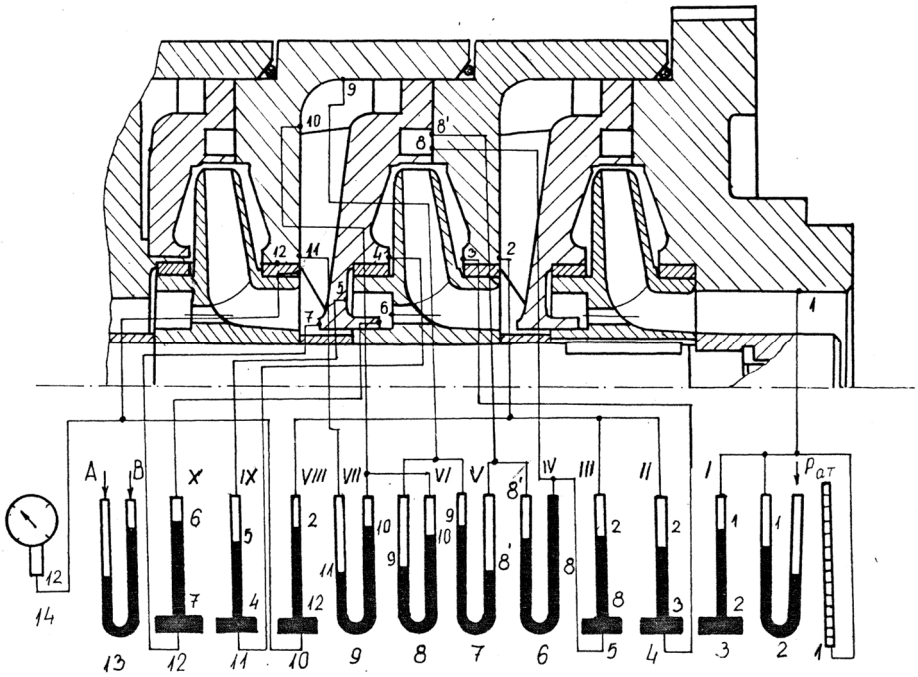

Figure 4. A diagram of the experimental setup (system). Reproduced with permission from Petrov, P.R. Investigation of the influence of the Radial diffuser and the return guide vanes on the performance of a multistage centrifugal pump. PhD thesis published by the University of Ruse, Ruse, Bulgaria, 1983.

2.7. Validation of Numerical Results

After performing numerical simulations, using Mesh1.2 and Transient Blade Row, the values for the pump stage flow rate Q, head H, and hydraulic efficiency coefficient η_H are obtained.

In Figure 5, the results obtained both experimentally and through numerical simulations are presented.

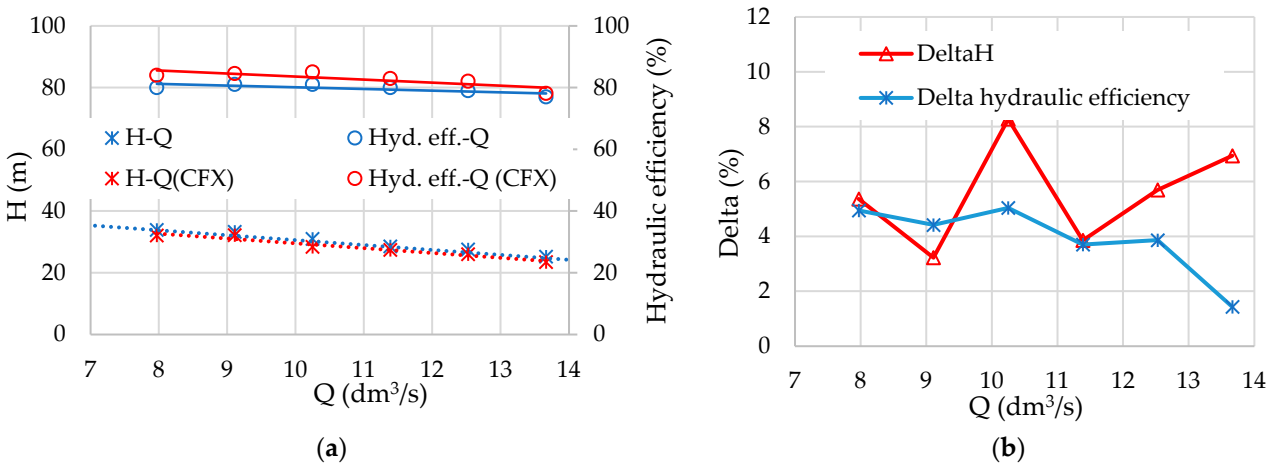

Figure 5. The validation of numerical results includes (**a**) relationships regarding the impact of flow rate on head and hydraulic efficiency, obtained through experimental methods (as seen in Ref. [2]) and numerical simulations; (**b**) relative errors δ_H and δ_η given as functions of the flow rate.

To evaluate the accuracy of the results obtained, the relative errors of the head δ_H and the hydraulic coefficient of efficiency δ_η are calculated by applying the following equations:

$$\delta_H = \frac{|H_{exp} - H_{CFX}|}{H_{exp}} 100\% \quad (11)$$

and

$$\delta_\eta = \frac{|\eta_{H,exp} - \eta_{H,CFX}|}{\eta_{H,exp}} 100\% \quad (12)$$

where H_{exp} and $\eta_{H,exp}$ are the values of head and hydraulic coefficient of efficiency obtained experimentally, while H_{CFX} and $\eta_{H,CFX}$ are obtained after performing numerical simulations.

In Figure 5b, the relationship demonstrating the impact of the flow rate on the relative errors (deviations) δ_H and δ_η is presented. The largest relative error of the head reaches 8%, and the hydraulic coefficient of efficiency is 5%. According to Ref. [1], p. 614, for academic studies with no commercial risk, the targeted tolerances on head and power may be limited to $\pm$10%.

3. Results and Discussion

As a result of the numerical experiments performed, using Mesh1.2, various relationships are obtained regarding the energy indicators (parameters) of the pump stage studied and the pump flow rate. Most of the results are presented in dimensionless (relative) form, where the dimensionless parameters are calculated using the following equations:

$$Q_{rel} = \frac{Q_i}{Q_n} \quad (13)$$

$$H_{rel} = \frac{H_i}{H_n} \quad (14)$$

$$h_{v,rel} = \frac{h_{v,i}}{h_{v,n}} \quad (15)$$

$$\eta_{H,rel} = \frac{\eta_{v,i}}{\eta_{v,n}} \quad (16)$$

where H_n, $h_{v,n}$ and $\eta_{i,n}$ are the values of the relevant parameters obtained while operating with the original RGV and flow rate $Q_n = 11.39$ dm^3/s.

Figure 6 represents the results obtained concerning the main operating parameters of the studied pump stage: relative head H_{rel}, relative theoretical head $H_{t.rel}$, relative total energy loss $h_{v,rel}$ and relative hydraulic coefficient of efficiency $\eta_{H,rel}$, given as a function of the relative flow rate Q_{rel}.

The theoretical head can be estimated using the following equation:

$$H_t = H + h_v \quad (17)$$

where the total energy loss in the pump stage is determined as follows:

$$h_v = h_{v,imP} + h_{v,diff} \quad (18)$$

The losses $h_{v,imP}$ in the studied impeller and those obtained in Radial diffuser 1 $h_{v,diff}$ are determined by applying Equation (9) after determining entropy production in the impeller and diffuser 1 according to the methods described in Section 2.4.

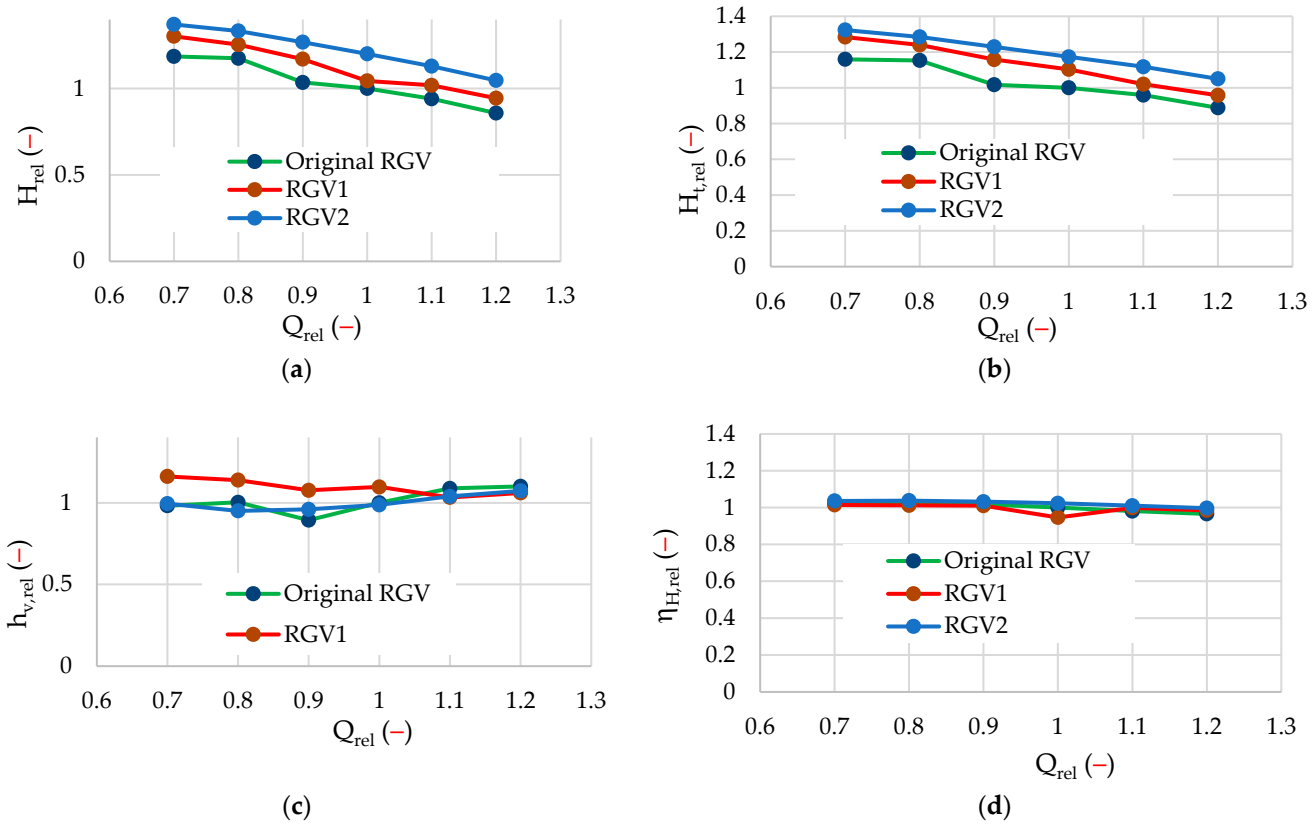

Figure 6. The results obtained after conducting numerical experiment include (**a**) the relationship between the relative head and the relative flow rate of the studied pump stage when operating with the three types of RGV; (**b**) the relationship between the relative theoretical head and the relative flow rate of the studied pump stage when operating with the three types of RGV; (**c**) the relationship between the relative total energy loss and the relative flow rate of the studied pump stage when operating with the three types of RGV; (**d**) the relationship between the relative hydraulic coefficient of efficiency and the relative flow rate of the studied pump stage when operating with the three types of RGV.

The analysis of the results presented in Figure 6 clearly indicates that when operating with RGV2, the head and theoretical head of the pump stage increase by nearly 20% compared to the original RGV. The values for RGV1 are between those obtained for RGV2 and the original RGV. The total energy losses and hydraulic coefficient of efficiency when operating with RGV2 and the original RGV differ slightly and are practically the same.

In Figure 7, relationships regarding different types of losses are presented. These losses are caused by entropy production in Impeller 2 and Radial diffuser 2. The symbols $h_{v,T}$, $h_{v,V}$ and $h_{v,W}$ are used to represent losses due to the velocity fluctuation, viscous diffusion and wall effect, respectively. By examining the graphs, it is evident that energy losses in the diffuser are predominant in all cases, with turbulent velocity fluctuation accounting for the largest share. The losses from viscous diffusion are minimal, and those came as a result while losses from friction on the walls correspond to the losses $h_{v,T}$.

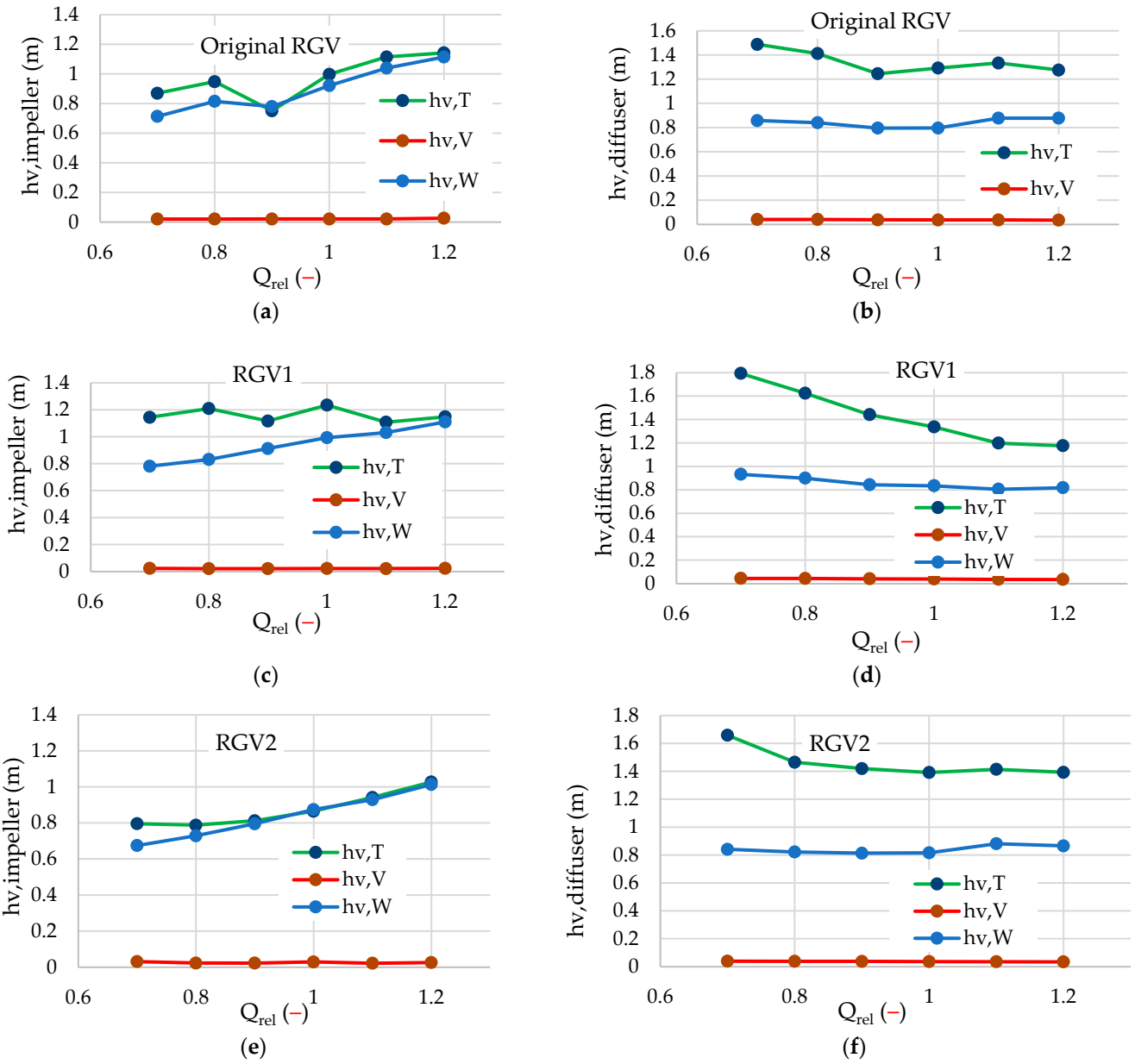

Figure 7. Losses incurred in the Impeller and Radial diffuser 1 due to entropy production. This includes (**a**) relationships pertaining to the three types of entropy production, where losses in the form of head are observed in Impeller 2 while operating with the original RGV; (**b**) relationships related to the three types of entropy production, where losses in the form of the head are observed in Radial diffuser 1 while operating with the original RGV; (**c**) relationships related to the three types of entropy production, where losses in the form of head are observed in Impeller 2 while operating with RGV1; (**d**) relationships related to the three types of entropy production, where losses in the form of the head are observed in Radial diffuser 1 while operating with RGV1; (**e**) relationships related to the three types of entropy production, where losses in the form of head are observed in Impeller 2 while operating with RGV2; (**f**) relationships related to the three types of entropy production, where losses in the form of the head are observed in Radial diffuser 1 while operating with RGV2.

In order to illustrate the impact of RGV on the losses in the pump stage, the relationships between the relative losses, described by Equation (15), and the relative flow rate when operating with the three types of RGV are presented in Figure 8.

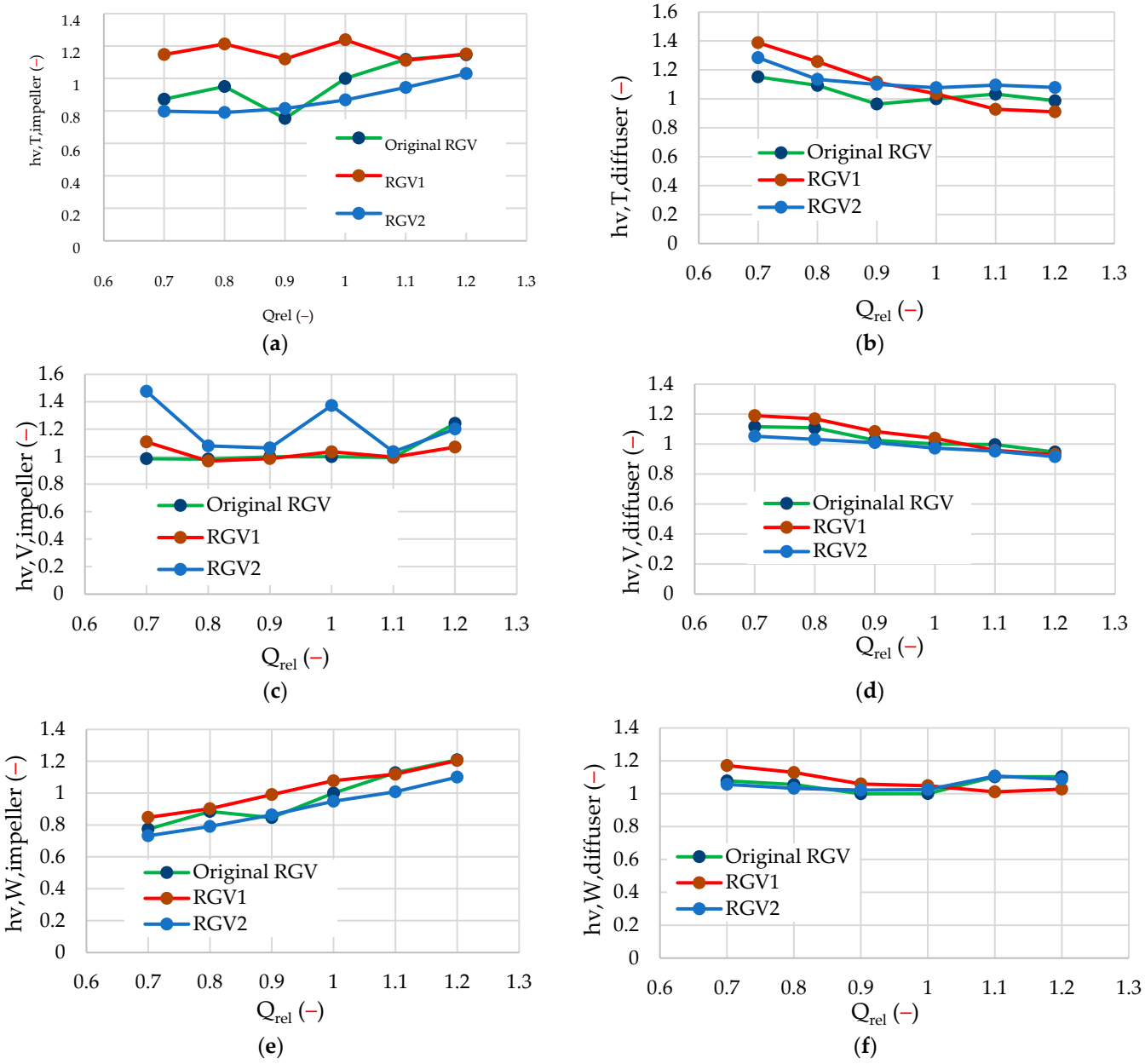

Figure 8. Relative losses in the Impeller and Radial diffuser 1 obtained as a result of entropy production. This includes (**a**) the relationships concerning the losses $h_{v,T}$, presented as head losses obtained in Impeller 2 when operating with the three types of RGV; (**b**) the relationships concerning the losses $h_{v,T}$, presented as head losses obtained in Radial diffuser 1 when operating with the three types of RGV; (**c**) the relationships concerning the losses $h_{v,V}$, presented as head losses obtained in Impeller 2 when operating with the three types of RGV; (**d**) the relationships concerning the losses $h_{v,V}$, presented as head losses obtained in Radial diffuser 1 when operating with the three types of RGV; (**e**) the relationships concerning the losses $h_{v,W}$, presented as head losses obtained in Impeller 2 when operating with the three types of RGV; (**f**) the relationships concerning the losses $h_{v,W}$, presented as head losses obtained in Radial diffuser 1 when operating with the three types of RGV.

The analysis of the graphs clearly indicates that in all cases, the losses $h_{v,T}$, $h_{v,V}$ and $h_{v,W}$ have similar values when the pump is operating with the original RGV and RGV2, which holds true for the entire range of flow rate studied. The loss values when operating with RGV1 fluctuate between those of RGV2 and the original RGV. Losses $h_{v,T}$ obtained

in the pump impeller predominate when operating with RGV1, while losses $h_{v,V}$ in the diffuser predominate when operating with RGV. When using the diffuser, the individual types of losses are similar when operating with the three studied vanes. Analyzing the previous statements leads to the conclusion that the shape (design) of the studied vanes does not have a significant impact on the losses in the pump stage, as well as on its hydraulic coefficient of efficiency.

In order to clarify the reason for the increased head when operating with vanes RGV1 and RGV2, the impact of RGV on the velocity field in front of Impeller 2, and thus on the theoretical head H_t, is studied.

To achieve the main purposes of this study, the theoretical head H_t and the head of Impeller 2 H_{imp} are determined by applying the following equations:

$$H_t = \frac{\overline{u_2 c_{u2}} - \overline{u_1 c_{u1}}}{g} \tag{19}$$

where $\overline{u_1 c_{u1}}$ and $\overline{u_2 c_{u2}}$ are mass flow averaged values, obtained by using the relative velocity $u = r\omega$ and the relevant component of the absolute velocity c_u (circumferential velocity) at the entrance (subscript 1) and at the impeller output (subscript 2); ω (rad/s) is the impeller angular velocity; r is the radius at the inlet and Outlet of the impeller; g is gravity acceleration.

In Figure 9, a velocity field of the absolute velocity $\vec{c}$ is presented in a cross-section located just before the inlet of Impeller 2. The impeller rotates counterclockwise.

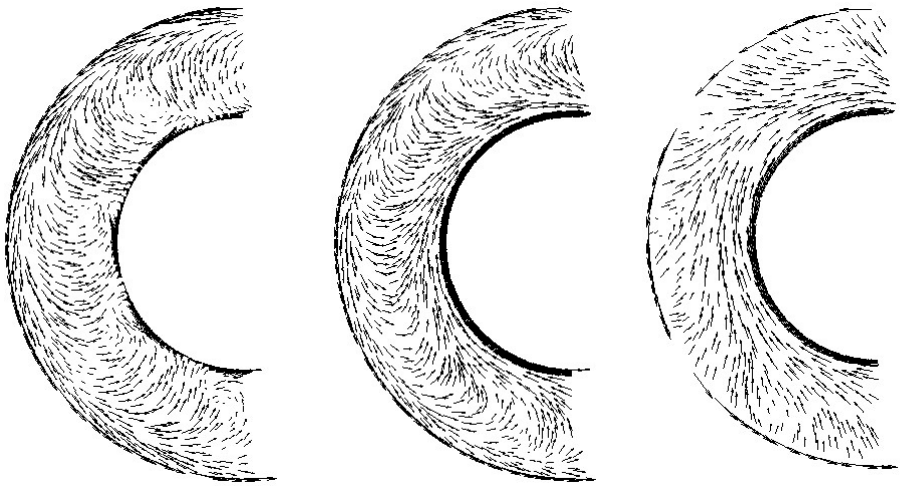

(**a**) (**b**) (**c**)

Figure 9. A velocity field of the absolute velocity $\vec{c}$ concerning a cross-section located just at the inlet of Impeller 2 being analyzed under the following conditions (**a**) when operating with the original RGV and flow rate Q = 11.39 dm^3/s; (**b**) when operating with RGV1 and flow rate Q = 11.39 dm^3/s; (**c**) when operating with RGV2 and flow rate Q = 11.39 dm^3/s.

In the presented figure, it can be observed that when operating with RGV2 (b), the vector field is mainly oriented in a direction opposite to the rotation of the impeller. This affects the value of circumferential velocity c_{u1}. To assess this impact, the value of $\overline{c_{u1}}$ is to be calculated—the mass flow averaged circumferential velocity in the studied cross-section. Figure 10 presents a relationship of the type $\overline{c_{u1}} = f(Q_{rel})$, which is obtained based on the results of CFD modeling.

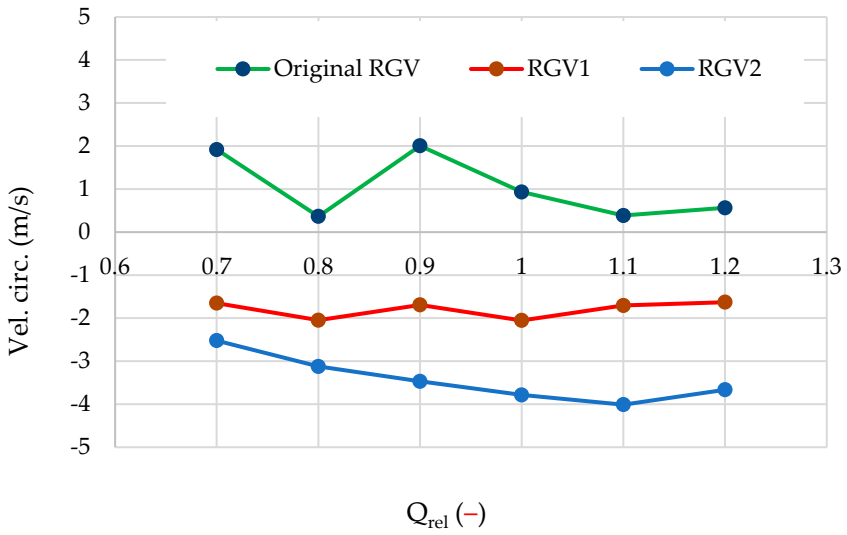

Figure 10. Relationships of mass flow averaged circumferential velocity are presented as a function of Q_{rel} , regarding the cross-section situated just before the inlet of Impeller 2, when operating with the three RGV.

The analysis of the relationships, presented graphically in Figure 10, clearly indicates that in all pump modes, when operating with the original RGV, $\overline{c_{u1}} > 0$. In the case of using RGV1 and RGV2 $\overline{c_{u1}} < 0$ in all cases studied, as, in addition $\overline{c_{u1}}$, it is observed that operating with RGV2 has a lower value (larger absolute value) than $\overline{c_{u1}}$, operating with RGV1. Based on the previous statement, in the authors' opinion, the impact of the RGV angle α_6 on the velocity distribution in front of the inlet of the next impeller can be seen, and thus also on the theoretical head of the studied impeller. When RGV has the largest angle (128 deg), $\overline{c_{u1}}$ has the lowest value, which, according to Equation (17), leads to an increase in head H_t. Since the shape (design) of the vane does not result in a significant increase in losses, this leads to obtaining a greater head H of the pump stage.

The impact of the RGV shape on the flow kinematics in front of the Impeller 2 inlet can also be observed in the results presented in Figure 11.

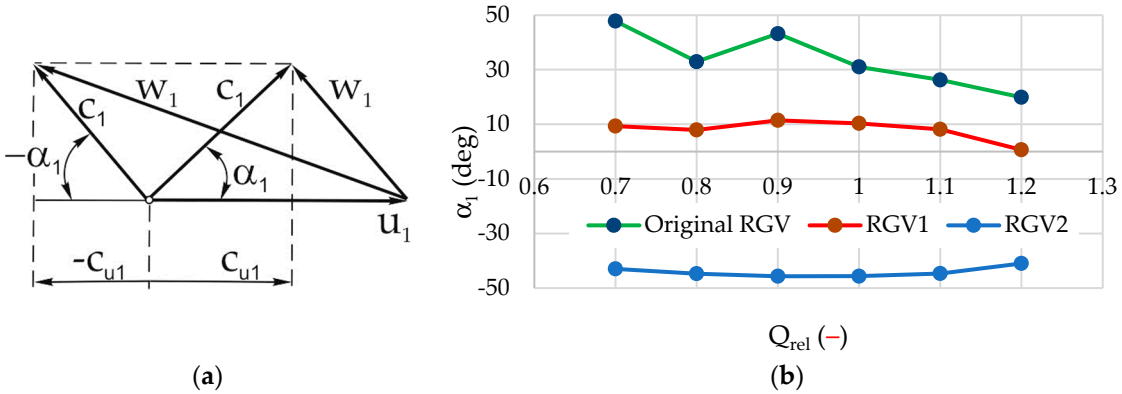

Figure 11. Impact of RGV on (**a**) velocity triangle in front of Impeller 2 inlet; (**b**) angle α_1 in the studied range of flow rates.

Figure 11a shows velocity triangles in front of the impeller inlet when the angle α_1 between the absolute velocity c_1 and the transition velocity u_1 has positive and negative values. It is well known that in the case of $\alpha_1 > 0$, the theoretical head of the pump stage is less than at $\alpha_1 < 0$. At the same time, negative values of α_1 lead to an increase in shock (kick) losses at the inlet of the impeller blades. In Figure 11b, the results obtained after performing numerical simulations for averaged angle (α_1) values in the section just in front

of the impeller inlet are presented when the studied pump stage operates with the three RGVs. It is clear that when operating with the original RGV, $\alpha_1 > 0$ for the entire range of studied flow rates. When operating with RGV1, $\alpha_1 > 0$, but takes lower values than when operating with the original RGV. Using RGV2 leads to $\alpha_1 < 0$ concerning the entire range of flow rates studied, resulting in the generation of the greatest head when this type of RGV is used.

4. Conclusions

In this study, we numerically examined the impact of the RGV of a stage in a two-stage pump on its indicators, including operating parameters such as head, losses and hydraulic coefficient of efficiency.

Three RGVs with different Outlet angles were studied: α_6—original RGV with $\alpha_6 = 90$ deg, RGV1 with $\alpha_6 = 110$ deg and RGV2 with $\alpha_6 = 128$ deg.

Based on the simulations conducted, the following key conclusions can be made:

- When operating with RGV2, the pump stage ensures nearly 20% more head than when operating with the original RGV;
- When operating with the three types of RGV, the head loss and hydraulic coefficient of efficiency obtained are practically the same;
- When operating with the three types of vanes, losses in the diffuser dominate over those in the impeller;
- Based on the entropy production analysis, it can be concluded that in all considered operating cases, losses due to velocity fluctuation dominate, and losses from viscous diffusion are insignificant. Losses resulting from wall friction are similar in value to those obtained due to velocity fluctuation;
- The impact of the larger angle α_6 on the head of the pump stage is expressed in the creation of a negative circulation relative to the axis of rotation in front of the impeller inlet, leading to its increase. In this sense, the original RGV creates a positive circulation, while RGV1 and RGV2 create a negative circulation, which is valid in all studied modes of pump stage operation.

Author Contributions: Conceptualization, K.K. and J.G.; methodology, G.P.; software, K.K. and J.G.; validation, B.K. and S.I.; formal analysis, J.G., K.K., G.P., B. K. and S.I.; investigation, S.I. and B. K.; resources, J.G. and K.K.; data curation, K.K., G.P. and B.K.; writing—original draft preparation, K.K., J.G. and G.P.; writing—review and editing, G.P.; visualization, K.K., B.K. and J.G.; supervision, K.K. and G.P.; project administration, S.I.; funding acquisition, J.G. and K.K. All authors have read and agreed to the published version of the manuscript.

Funding: This research was funded by the European Union–NextGenerationEU, through the National Recovery and Resilience Plan of the Republic of Bulgaria, project № BG-RRP-2.013-0001.

Institutional Review Board Statement: Not applicable.

Informed Consent Statement: Not applicable.

Data Availability Statement: The raw data supporting the conclusions of this article will be made available by the authors on request.

Conflicts of Interest: The authors declare no conflicts of interest.

References

1. Gülich, J. *Centrifugal Pumps*, 4th ed.; Springer: Cham, Switzerland, 2020.
2. Petrov, P.R. Investigation of the Influence of the Radial Diffuser and the Return Guide Vanes on the Performance of a Multistage Centrifugal Pump. Ph.D. Thesis, University of Ruse, Ruse, Bulgaria, 1983.
3. La Roche-Carrier, N.; Ngoma, G.N.; Ghie, W. Numerical Investigation of Liquid Flow in Two-, Three- and Four-Stage Centrifugal Pumps. In Proceedings of the 4th International Conference on Simulation and Modeling Methodologies, Technologies and Applications (SIMULTECH-2014), Vienna, Austria, 28–30 August 2014.
4. Zhang, Q.; Shi, W.; Xu, Y.; Gao, X.; Wang, C.; Lu, W.; Ma, D. A new proposed return guide vane for compact multistage centrifugal pumps. *Int. J. Rotating Mach.* **2013**, *2013*, 683713. [CrossRef]

5. Zhai, L.; Lu, C.; Guo, J.; Cui, B. Flow characteristics and energy loss of a multistage centrifugal pump with blade-type guide vanes. *Mar. Sci. Eng.* **2022**, *10*, 180. [CrossRef]
6. Miyano, M.; Kanemoto, T.; Kawashima, D.; Wada, A.; Hara, T.; Sakoda, K. Return vane installed in multistage centrifugal pump. *Int. J. Fluid Mach. Syst.* **2008**, *1*, 57–63. [CrossRef]
7. Zhang, Q.H.; Xu, Y.; Shi, W.D.; Lu, W.G. Research and development on the hydraulic design system of the guide vanes of multistage centrifugal pumps. In Proceedings of the IOP Conference Series: Earth and Environmental Science: 26th IAHR Symposium on Hydraulic Machinery and Systems, Beijing, China, 19–23 August 2012.
8. Wang, C.; Shi, W.; Wang, X.; Jiang, X.; Yang, Y.; Li, W.; Zhou, L. Optimal design of multistage centrifugal pump based on the combined energy loss model and computational fluid dynamics. *Appl. Energy* **2017**, *187*, 10–26. [CrossRef]
9. Kim, D.; Mamatov, S.; Jeon, S.; Park, W. A study of the performance of a radial diffuser for a multistage high-pressure pump. *J. Mech. Sci. Technol.* **2017**, *31*, 1693–1700. [CrossRef]
10. Wu, D.; Yao, S.; Lin, R.; Ren, Y.; Zhou, P.; Gu, Y.; Mou, J. Dynamic instability analysis of a double-blade centrifugal pump. *Appl. Sci.* **2021**, *11*, 8180. [CrossRef]
11. Rao, Z.; Tang, L.; Zhang, H. Double-tongue worm shell structure on plastic centrifugal pump performance study. *Appl. Sci.* **2023**, *13*, 8507. [CrossRef]
12. Babayigit, O.; Ozgoren, M.; Aksoy, M.; Kocaaslan, O. Experimental and CFD investigation of a multistage centrifugal pump including leakages and balance holes. *Desalin. Water Treat.* **2017**, *67*, 28–40. [CrossRef]
13. La Roche-Carrier, N.; Ngoma, G.N.; Ghie, W. Effects of Wall Roughness, Impeller Blades and Diffuser Vanes on the Performances of a First Stage Centrifugal Pump. In Proceedings of the 3rd International Conference on Simulation and Modeling Methodologies, Technologies and Applications (SIMULTECH-2013), Reykjav'ik, Iceland, 29–31 July 2013.
14. La Roche-Carrier, N.; Ngoma, G.N.; Ghie, W. Numerical Investigation of a First Stage of a Multistage Centrifugal Pump: Impeller, Diffuser with Return Vanes, and Casing. *ISRN Mech. Eng.* **2013**, *2013*, 578072. [CrossRef]
15. He, X.; Jiao, W.; Wang, C.; Cao, W. Influence of surface roughness on the pump performance based on computational fluid dynamics. *IEEE Access* **2019**, *7*, 105331–105341. [CrossRef]
16. Shamsuddeen, M.; Ma, S.-B.; Kim, S.; Yoon, J.-H.; Lee, K.-H.; Jung, C.; Kim, J.-H. Effect of an inducer-type guide vane on hydraulic losses at the inter-stage flow passage of a multistage centrifugal pump. *Processes* **2021**, *9*, 526. [CrossRef]
17. Lee, J.; Moshfeghi, M.; Hur, N.; Yoon, I. Flow analysis in a return channel of a multi-stage centrifugal pump. *J. Mech. Sci. Technol.* **2016**, *30*, 3993–4000. [CrossRef]
18. Zhao, W.; Hu, J.; Wang, K. Influence of channel-diffuser blades on energy performance of a three-stage centrifugal pump. *Symmetry* **2021**, *13*, 277. [CrossRef]
19. Lin, T.; Li, X.; Zhu, Z.; Xie, J.; Li, Y.; Yang, H. Application of enstrophy dissipation to analyze energy loss in a centrifugal pump as turbine. *Renew. Energy* **2020**, *163*, 41–55. [CrossRef]
20. Hou, H.; Zhang, Y.; Li, Z.; Jiang, T.; Zhang, J.; Xu, C. Numerical analysis of entropy production on a LNG cryogenic submerged pump. *J. Nat. Gas Sci. Eng.* **2016**, *36*, 87–96. [CrossRef]
21. Shu, Z.; Shi, G.; Yao, X.; Sun, G.; Tao, S. Influence factors and prediction model of enstrophy dissipation from the tip leakage vortex in a multiphase pump. *Sci. Rep.* **2022**, *12*, 16032. [CrossRef] [PubMed]
22. Li, H.; Chen, Y.; Yang, Y.; Wang, S.; Bai, L.; Zhou, L. CFD Simulation of Centrifugal Pump with Different Impeller Blade Trailing Edges. *J. Mar. Sci. Eng.* **2023**, *11*, 402. [CrossRef]
23. Ji, L.; Li, W.; Shi, W.; Tian, F.; Agarwal, R. Effect of blade thickness on rotating stall of mixed-flow pump using entropy generation analysis. *Energy* **2021**, *236*, 121381. [CrossRef]
24. Kock, F.; Herwig, H. Local entropy production in turbulent shear flows: A high-Reynolds number model with wall functions. *Int. J. Heat Mass Transf.* **2004**, *47*, 2205–2215. [CrossRef]
25. Kock, F.; Herwig, H. Entropy production calculation for turbulent shear flows and their implementation in cfd codes. *Int. J. Heat Mass Transf.* **2005**, *26*, 672–680. [CrossRef]